THE AMERICAN SOCIETY OF MECHANICAL ENGINEERS
345 E. 47th St., New York, N.Y. 10017

96-GT-335

A MODAL COUPLING FOR FLUID AND STRUCTURE ANALYSES OF TURBOMACHINE FLUTTER. APPLICATION TO A FAN STAGE.

Francois Moyroud[†]*, Georges Jacquet-Richardet* and Torsten Fransson[†]

[†] Chair of Heat and Power Technology
Royal Institute of Technology
S-10044 Stockholm, Sweden

* Laboratoire de Mécanique des Structures, U.R.A. C.N.R.S. 862
Institut National des Sciences Appliquées
F-69621 Villeurbanne, France

ABSTRACT

The paper presents an approach for the modal aeroelastic analysis of three-dimensinnal turbomachinery bladings with several fluid and structure analyzers. Structure analyzers are three-dimensional solvers for static and dynamic analyses of axisymmetric/cyclic-symmetric blade-shroud-disk-shaft assemblies with/without elastic coupling between blades. Fluid analyzers are two-dimensional/three-dimensional solvers for single/multi-stage steady/unsteady turbomachinery flows. An automatic interfacing procedure for exchanging data at the incompatible fluid-structure boundary and the development of a multi-model interfacing software are discussed. The modal aeroelastic analysis of a first stage shrouded fan is carried out to illustrate the main issues of the paper. In particular, two structural models for the elastic coupling of the part-span shrouds are discussed. The results show the strong dependence of the structure dynamics and aeroelastic analysis on this modelling.

Nomenclature

Latin Alphabet

MAP	Mean Accumulated Power
N	Number of blades on the rotor
OP	Aerodynamic Operating Point
$\{\bar{F}\}$	Vector of steady aerodynamic forces
$\{\tilde{F}\}$	Vector of motion dependent aerodynamic forces
j	Imaginary unit ($j^2 = -1$)
n	Travelling wave number ($n=0,...,N$)
$\{\hat{q}(t,\beta_n)\}$	Vector of time-dependent generalized coordinates
$\{\hat{q}(\beta_n)\}$	Generalized coordinates harmonic amplitudes

Greek Alphabet

β_n	Travelling wave propagation constant
$\{\delta\}$	Vector of static displacements
$\{\hat{\delta}(t)\}$	Vector of dynamic displacements
λ^*_{a,β_n}	Aeroelastic eigenvalue
ω_{a,β_n}	Structure natural eigenfrequency
ω^*_{a,β_n}	Aeroelastic eigenfrequency
Ω	Rotor speed
μ_{a,β_n}	Aerodynamic damping [Carta; 1967] (aerodynamic work per cycle divided by mean kinetic energy over one cycle)
μ^*_{a,β_n}	Aeroelastic eigendamping

Superscripts

$*$	Complex conjugate
T	Matrix/vector transpose
$\Re$	Real part
$\Im$	Imaginary part

Sign Convention

positive (negative) n corresponds to forward (backward) waves. positive (negative) aeroelastic/aerodynamic damping ratios correspond to unstable (stable) modes.

1.0 INTRODUCTION AND OBJECTIVES

Considerable progress has been accomplished in the development of computational methods for single-field problems in turbomachines such as structural or fluid dynamics. Since the development of techniques for coupled-field problems requires multidisciplinary expertise, it has understandably lagged behind. Recently, design requirements for efficient use of material resources, emphasis on energy-efficient design and concerns for equipment safety have boosted the demand for realistic computer analyses of fluid-structure interactions in turbomachines.

To date fluid-structure interactions have been tackled, either in the frequency domain or in the time domain [Bendiksen; 1990]:

Presented at the International Gas Turbine and Aeroengine Congress & Exhibition
Birmingham, UK — June 10-13, 1996

- *Frequency domain* is a natural setting for structural, aerodynamic and aeroelastic problems amenable to Fourier-type solutions.
- *Time domain* is a natural setting for nonlinear problems.

Linearized and frequency domain approaches have played and still play a primary role in aeroelastic simulations [Kielb and Kaza; 1984] [Srinivasan and Fabunmi; 1984] [Henry and Vincent; 1990] [Smith; 1991] [Gerolymos; 1993] [Jacquet-Richardet and Henry; 1994] [Imregun; 1995].

Despite the growth of computer performances and algorithm developments, time dnmain solution procedures are, in general, resource intensive and largely in formative stage for turbomachinery flutter [Bendiksen; 1991; 1994] [He; 1994] [Vadhati and Imregun; 1994] [Marshall and Imregun;1995]. Although they certainly can benefit from parallel processing technology, they are currently computationally expensive for design procedures.

Aeroelastic coupling procedures should be accurate with the least computer time consumed. They also need to be devised so as to allow the analyst to select one or several structure and fluid analyzers that best fit the problem at hand. For example, the most accurate numerical model cannot be used if it is not available on time in a design procedure. So clearly the range of analyzers should go from models which are acceptably accurate and fast to those which are highly accurate but computer time consuming.

There are several advantages in the development and use of coupled field software supporting arbitrary single-field analyzers:

1. It is cost efficient to use the bulk of existing single-field engineering analyzers that have been independently developed and validated.
2. As problems arise, such software can be easily augmented to include new single-field analyzers or additional effects with minimum time of development.

The modal aeroelastic analysis scheme previously discussed, for example, by Srinivasan and Fabunmi [1984], Henry and Vincent [1990], Smith [1991] Gerolymos [1993], Jacquet-Richardet and Henry [1994], is used in this work. It is augmented with additional features for using *several structure* and *fluid analyzers* within a single fluid-structure coupling program. Structure analyzers are advanced three-dimensional solvers for the static and dynamic analysis of axisymmetric/cyclic-symmetric blade-shroud-disk-shaft assemblies with/without elastic coupling between blades. Fluid analyzers are advanced two-dimensional/three-dimensional solvers for single/multi-stage steady/unsteady turbomachinery flows. The main contribution of this work are: (a) the discussion of some relevant computational issues with the modal aeroelastic analysis scheme (b) the development of an automatic interfacing procedure for exchanging data at the incompatible fluid-structure boundary, (c) the discussion of the development of the resulting multi-model interfacing software, and (d) the demonstration of the proposed aeroelastic analysis procedure for a first-stage shrouded fan.

2.0 THEORETICAL BACKGROUND

When modelling the statics and dynamics of modern turbomachinery rotors, elastic coupling between individual elements (blade, part-span or tip shrouds, disk, shaft) and aeroelastic coupling should be accounted for. The governing equations of motion of such blade-shroud-disk-shaft assemblies based on a finite element discretisation scheme are:

$$[M]\{\ddot{\delta}(t)\} + [C(\Omega)]\{\dot{\delta}(t)\} + \overbrace{\left[K_L + K_{NL} - \Omega^2 M_G\right]}^{K}\{\delta(t)\} - \{\bar{F}_c(\Omega)\} = \{\bar{F}(OP)\} + \{\hat{F}(OP, t, \delta(t), \ldots)\} \quad \text{(EQ 1)}$$

On the left hand side, the structural equations of motion contain: $\{\delta(t)\}$ the state vector of the total structural displacements, $[M]$ the spatial mass matrix, $[C(\Omega)]$ the spatial gyroscopic matrix, $[K]$ the spatial nonlinear stiffness matrix including stress stiffening and spin softening, and $\{\bar{F}_c(\Omega)\}$ the state vector of centrifugal forces. The structural damping is neglected. On the right hand side are the state vectors of the steady $\{\bar{F}(OP)\}$ and unsteady motion dependent $\{\hat{F}(OP, t, \delta(t), \ldots)\}$ aerodynamic forces.

Equation (1) is in general nonlinear. In this work, the solution is obtained in two steps:

1. First, all time dependent terms are discarded. This leads to the nonlinear static problem, the solution of which is the static equilibrium state $\{\bar{\delta}\}$ of the structure under centrifugal and steady aerodynamic loading:

$$[K]\{\bar{\delta}\} - \{\bar{F}_c(\Omega)\} = \{\bar{F}(OP)\} \quad \text{(EQ 2)}$$

   (EQ2) is nonlinear since the stiffness matrix includes geometric nonlinearities.
2. Second, all time dependent terms are reintroduced and the displacement state vector $\{\delta(t)\}$ replaced by a small perturbation $\{\tilde{\delta}(t)\}$ around the nonlinear static equilibrium state $\{\bar{\delta}\}$, which leads to:

$$[M]\{\ddot{\tilde{\delta}}(t)\} + [C(\Omega)]\{\dot{\tilde{\delta}}(t)\} + [K]\{\tilde{\delta}(t)\} = \{\hat{F}(OP, t, \tilde{\delta}(t), \ldots)\} \quad \text{(EQ 3)}$$

and

$$\{\delta(t)\} = \{\bar{\delta}\} + \{\tilde{\delta}(t)\}. \quad \text{(EQ 4)}$$

For solving (EQ 2) and (EQ 3), current modelling consist in splitting the structure and fluid computational domains into perfectly identical (tuned rotor) or nearly identical (mistuned rotor) subdomains (one substructure and one fluid passage). The solution is then expressed in terms of N travelling wave modes or coordinates (see for example [Crawley; 1984] [Kaza and Kielb; 1984]).

To simplify the notations, the parameter OP will be omitted in the rest of the text. However, it is clear that the solution is a function of the aerodynamic operating point of the turbomachine.

2.1 Travelling Waves

For an N-bladed rotor, the blade displacements $\{\tilde{\delta}(t)\}_s$, the fluid state vector and the motion dependent forces $\{\hat{F}(t, \tilde{\delta}(t), \ldots)\}_s$ attached to the subdomain s (s=1,...,N) are expressed in terms of travelling wave coordinates attached to a reference subdomain 1:

$$\{\tilde{\delta}(t)\}_s = \sum_{n=0}^{N-1} \{\hat{\tilde{\delta}}(t, \beta_n)\}_1 e^{j(s-1)\beta_n}. \quad \text{(EQ 5)}$$

$$\{\hat{F}(t,\tilde{\delta}(t),\ldots)\}_s = \sum_{n=0}^{N-1} \{\hat{F}\left(t,\hat{\delta}\left(t,\beta_n\right),\ldots,\beta_n\right)\}_1 e^{j(s-1)\beta_n} \quad \text{(EQ 6)}$$

The travelling wave constant β_n satisfies the cyclic symmetric condition:

$$N\beta_n = 2\pi n \text{ for every } n=0,N\text{-}1. \quad \text{(EQ 7)}$$

The introduction of the travelling waves transformation into (EQ 3) leads to the following dynamic equations [Jacquet-Richardet; 1994]:

$$[\tilde{M}]\{\ddot{\hat{\delta}}(t)\} + [\tilde{C}(\Omega)]\{\dot{\hat{\delta}}(t)\} + [\tilde{K}]\{\hat{\delta}(t)\} = \{\hat{F}\left(t,\hat{\delta}(t),\ldots\right)\}. \quad \text{(EQ 8)}$$

Case 1: If the structure and/or the fluid are/is mistuned, the travelling waves are coupled. If D is the number of degrees of freedom per substructure then $[\tilde{M}]$, $[\tilde{C}(\Omega)]$, $[\tilde{K}]$ are $D\times N\times D\times N$ matrices, and:

$$\{\hat{\delta}(t)\} = \left[\{\hat{\delta}\left(t,\beta_1\right)\}_1 \ldots \{\hat{\delta}\left(t,\beta_n\right)\}_1 \ldots \{\hat{\delta}\left(t,\beta_N\right)\}_1\right]^T \quad \text{(EQ 9)}$$

$$\{\hat{F}\left(t,\hat{\delta}(t)\right)\} = \left[\{\hat{F}\left(t,\hat{\delta}\left(t,\beta_1\right),\ldots,\beta_1\right)\}_1 \ldots\ldots \{\hat{F}\left(t,\hat{\delta}\left(t,\beta_N\right),\ldots,\beta_N\right)\}_1\right]^T$$

For any arbitrary distributions of mistuning, the travelling wave decomposition does not lead to any reduction in size of the system of equations.

Case 2: If the structure and the fluid are tuned, the system matrices are sized down to $D\times D$ terms. The travelling waves are uncoupled and (EQ 8) splits into N independent subsystems ($n=1,\ldots,N$):

$$[\tilde{M}]_1\{\ddot{\hat{\delta}}\left(t,\beta_n\right)\}_1 + [\tilde{C}(\Omega)]_1\{\dot{\hat{\delta}}\left(t,\beta_n\right)\}_1 + [\tilde{K}]_1\{\hat{\delta}\left(t,\beta_n\right)\}_1 = \{\hat{F}\left(t,\hat{\delta}\left(t,\beta_n\right),\ldots,\beta_n\right)\} \quad \text{(EQ 10)}$$

Now, depending on whether the elastic coupling between substructures is accounted for, spatial matrices of (EQ 10) may or may not be functions of the phase constant β_n.

2.2 Modal Analysis

A direct solution of (EQ 8) in the time domain (by simultaneously or sequentially advancing the fluid equations in time) may be tedious for several reasons:

1. For realistic structural and fluid analyses, the number of equations is large enough to be computationally cumbersome.
2. If several fluid and solid analyzers are to be used, different numerical time integration schemes and spatial discretisation schemes for the fluid and the structure should be handled.
3. Fluid and solid computational domains should be matched at the nonconforming and/or incompatible coupled boundary for all time steps.

For linear structures, these points can be efficiently overcome using a modal decomposition of the coupled displacements. For a given set of M orthogonal structural mode shapes $[\tilde{\Phi}]$ and generalized coordinates $\{\hat{q}(t)\}$, the motion of the fluid-structure coupled system is expressed as:

$$\{\hat{\delta}(t)\} = [\tilde{\Phi}]\{\hat{q}(t)\} \quad \text{(EQ 11)}$$

It is convenient to use mode shapes of either the undamped non rotating structure or the undamped rotating structure without gyroscopic effect ($m=1,\ldots,M$):

$$\omega^2[\tilde{M}]\{\tilde{\Phi}_m\} + [\tilde{K}]\{\tilde{\Phi}_m\} = \{0\} \quad \text{(EQ 12)}$$

The resulting eigenmodes $[\tilde{\Phi}]$ are complex and the eigenvalues are real. The modal mass matrix and stiffness are real and diagonal:

$$[\tilde{m}] = [\tilde{\Phi}]^{*T}[\tilde{M}][\tilde{\Phi}] \in \Re \quad \text{(EQ 13)}$$
$$[\tilde{k}] = [\tilde{\Phi}]^{*T}[\tilde{K}][\tilde{\Phi}] \in \Re$$

Substituting (EQ 11) in (EQ 8) leads to:

$$[\tilde{m}]\{\ddot{\hat{q}}(t)\} + [\tilde{c}]\{\dot{\hat{q}}(t)\} + [\tilde{k}]\{\hat{q}(t)\} = \{\hat{U}\left(t,\{\hat{q}(t)\},\ldots\right)\} \quad \text{(EQ 14)}$$

where:

$$[\tilde{c}] = [\tilde{\Phi}]^{*T}[\tilde{C}][\tilde{\Phi}] \in C$$

$$\{\hat{f}\left(t,\{\hat{q}(t)\},\ldots\right)\} = [\tilde{\Phi}]^{*T}\{\hat{F}\left(t,\{\hat{\delta}(t)\},\ldots\right)\} \in C$$

The modal model (EQ14) has tremendous advantages compared to the spatial model (EQ8):

1. It leads to very small systems of equations (of size $M\times M << N\times N$),
2. The problem of handling arbitrary fluid-structure interface is basically solved since modal quantities are mesh independent.

3.0 COMPUTER IMPLEMENTATION

In the remaining of the paper we will be concerned with tuned cyclic symmetric rotors with elastic coupling.

3.1 Structure and Fluid Analyzers

In the frequency domain analysis, the vector of generalized coordinates $\{\hat{q}\left(t,\beta_n\right)\}$ is assumed to he a single harmonic function of time:

$$\{\hat{q}\left(t,\beta_n\right)\} = \{\hat{q}\left(\beta_n\right)\}e^{\lambda^*_{\beta_n} t} \quad \text{(EQ 15)}$$

Linear harmonic fluid analyzers assume that the fluid state vector (therefore the blade surface aerodynamic forces) is a linear function of the blade displacements. This is represented as:

$$\hat{U}\left(t,\{\hat{q}\left(t,\beta_n\right),\beta_n\}\right) = [\tilde{\Phi}]^{*T}\{\hat{F}\left(t,[\tilde{\Phi}]\{\hat{q}\left(t,\beta_n\right)\},\beta_n\right)\}$$
$$= [\tilde{\Phi}]^{*T}\left[\tilde{A}\left(\lambda^*_{\beta_n},[\tilde{\Phi}],\beta_n\right)\right]\{\hat{q}\left(\beta_n\right)\}e^{\lambda^*_{\beta_n} t} \quad \text{(EQ 16)}$$
$$= \left[\tilde{a}\left(\lambda^*_{\beta_n},[\tilde{\Phi}],\beta_n\right)\right]\{\hat{q}\left(\beta_n\right)\}e^{\lambda^*_{\beta_n} t}$$

$[\tilde{a}]$ is the $M\times M$ (unsymmetric complex) modal aerodynamic damping matrix, calculated from M structure mode shapes $[\tilde{\Phi}]$ obtained from (EQ 12). $\pi\tilde{a}^S_{l,m}$ may be interpreted as an aerodynamic work per cycle calculated with the mode shape No. l and the aerodynamic forcing function of mode shape No. m.

Although nonlinear fluid analyzers can also be used with harmonic motions, only the first harmonic of aerodynamic forces should be used to calculate the modal aerodynamic damping matrix. Furthermore, the mode shapes should be scaled so as to give sufficiently small amplitudes of vibration as input to the flow solver.

Although three-dimensional aerodynamic analyses have been proved necessary for steady and unsteady turbomachinery flows [Hall and Lorence; 1993] [Gerolymos and Vallet; 1994], it is also convenient to use a strip theory. In the latter case, two-dimensional analyses are stacked in the blade span-wise direction for a sufficient number of streamsurfaces

3.2 Modal Aeroelastic Coupling

Substituting (EQ 15) and (EQ 16) in (EQ 14) leads to the modal aeroelastic equations in the frequency domain:

$$\lambda^{*2}_{\beta_n}\left[\tilde{m}\left(\beta_n\right)\right]\{\hat{\tilde{q}}\left(\beta_n\right)\}+\lambda^{*}_{\beta_n}\left[\tilde{c}\left(\beta_n\right)\right]\{\hat{\tilde{q}}\left(\beta_n\right)\}+ \\ +\left[\tilde{k}\left(\beta_n\right)-\tilde{a}\left(\lambda^{*}_{\beta_n},\left[\tilde{\Phi}\right],\beta_n\right)\right]\{\hat{\tilde{q}}\left(\beta_n\right)\}=\{0\} \qquad \text{(EQ 17)}$$

The structure matrices $[\tilde{m}]$ and $[\tilde{k}]$ are hermitian, the aerodynamic matrix $[\tilde{a}]$ and gyroscopic matrix $[\tilde{c}]$ are not. The aeroelastic eigenvalues and eigenmodes are complex, i.e. damped system. Forward and backward aerodynamic and therefore aeroelastic travelling waves are not, in general, symmetric.

Since the aerodynamic damping matrix is a function of the aeroelastic eigenvalue, theoretically the problem should be solved with the iteration scheme shown in Fig. 1. The initial conditions to he analyzed are set by the natural mode (a,β_n). At every iteration, the aeroelastic frequency and damping ratio are given by:

$$\omega^{*}_{a,\beta_n}=\lambda^{*\Im}_{a,\beta_n} \text{ and } \mu^{*}_{a,\beta_n}=\frac{\lambda^{*\Re}_{a,\beta_n}}{\sqrt{\left(\lambda^{*\Re}_{a,\beta_n}\right)^2+\left(\lambda^{*\Im}_{a,\beta_n}\right)^2}} \qquad \text{(EQ 18)}$$

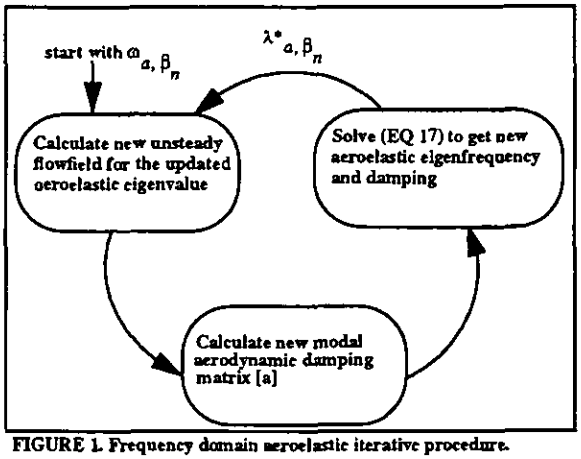

FIGURE 1. Frequency domain aeroelastic iterative procedure.

In practice, as shown in the numerical example, a very small number of iterations is sufficient for conventional metal blades. A larger number of iterations might be relevant for composite blades.

3.3 Non-Matching Fluid-Structure Interface Boundary

In general, the fluid and structure meshes have two independent representations of the physical fluid-structure interface $\Gamma_{F/S}$ (Fig. 2). When these representations are identical—that is, when every fluid point on that surface is also a structural node and vice-versa—the evaluation of the pressure forces and the transfer of the structural motion to the fluid mesh become trivial operations. However, analysts usually like to be able to:

- use different elements—quadrilaterals, pyramids, triangles, beams, etc.— for the fluid G_a and structure G_s meshes,
- refine each mesh independently from the other, and
- use fluid and structure meshes that have been independently designed and validated.

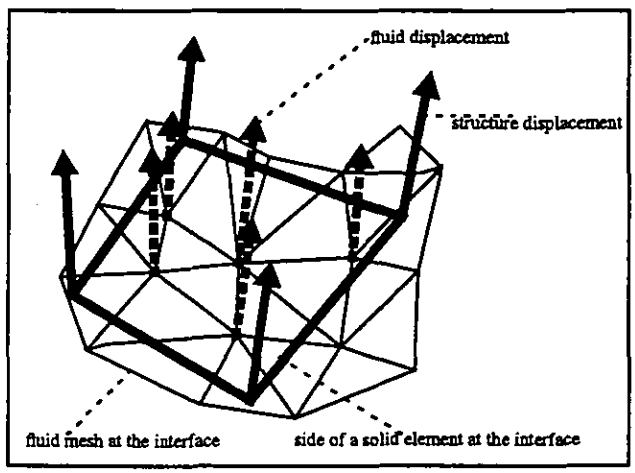

FIGURE 2. Three-dimensional non-matching fluid-structure interface boundary.

For aeroelastic analysis of wings numerous schemes have been proposed for smooth data (See, for example, the literature review by Appa [1989]). The present approach applies to turbomachinery blading and uses a three-dimensional interfacing grid G_i at the fluid-structure boundary. The shape functions nf the linear triangular plate finite element (T3) are used for interpolation and integration. The method is able to process in three-dimension *real/complex* and *smooth/irregular data* —mode shapes, steady/unsteady pressures—. It provides user's convenience and accuracy if G_i is as refined as the (blade surface) aerodynamic mesh G_a.

The following algorithm is used for transferring data:

1. Fluid mesh points at the boundary $\Gamma_{F/S}$ are located on G_a.
2. Structure mesb points at the boundary $\Gamma_{F/S}$ are located on G_s.
3. Fluid state variables are interpolated from G_a onto G_i.
4. Structure mode shapes are interpolated from G_s onto G_i.

The modal displacements and pressure distributions over the elements of G_i are given by:

$$\vec{\hat{\Phi}}^{e}_{l}\left(\xi_1,\xi_2,\xi_3\right)=\langle N\left(\xi_1,\xi_2,\xi_3\right)\rangle\{\hat{\Phi}_l\}^{e}$$
$$\hat{\hat{P}}^{e}_{m}\left(\xi_1,\xi_2,\xi_3\right)=\langle N\left(\xi_1,\xi_2,\xi_3\right)\rangle\{\hat{\hat{P}}_m\}^{e} \qquad \text{(EQ 19)}$$
$$1\le l,m\le M$$

where $\langle N \rangle$ are the element shape functions, $\{\tilde{\Phi}_l\}^e$ are the nodal values of mode shape l and $\{\hat{\tilde{P}}_m\}^e$ are the nodal values of unsteady pressures calculated for mode shape $\{\tilde{\Phi}_m\}^e$ at the aeroelastic eigenvalue λ^*_{a,β_n}.

The terms of the modal aerodynamic damping matrix (EQ 16) are given by:

$$\tilde{a}_{lm}\left(\lambda^*_{a,\beta_n}, [\tilde{\Phi}], \beta_n\right) = \sum_{e \in G_i} \iint_e -\vec{\tilde{\Phi}}_l^{\,e} \cdot \hat{\tilde{P}}_m^e \vec{n} \, dS \qquad \text{(EQ 20)}$$

$1 \le l, m \le M$

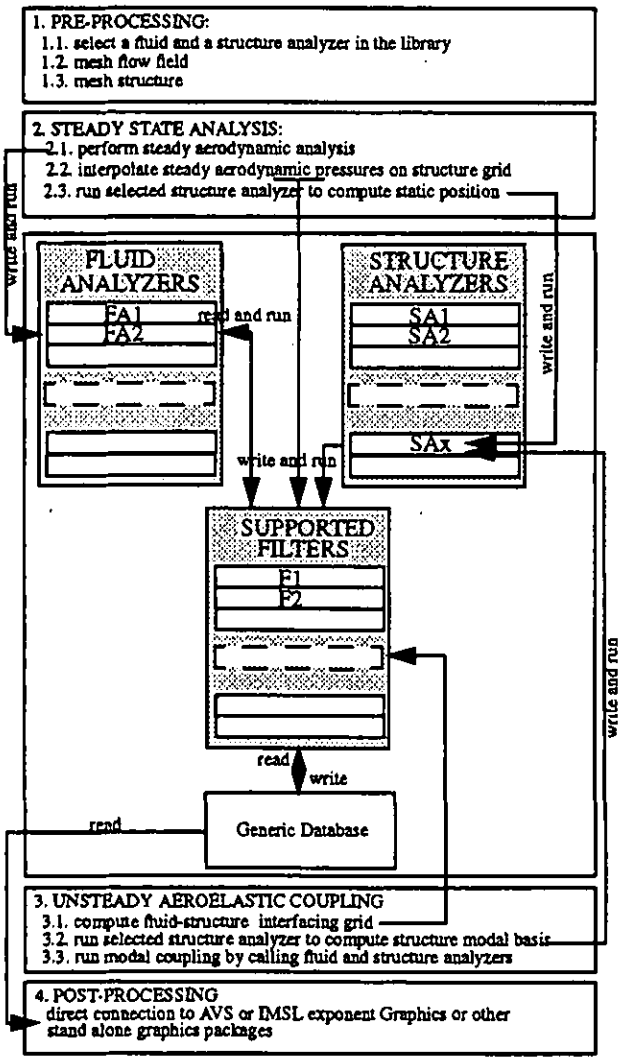

FIGURE 3. Short description of the computer architecture of STRUFLO (Korn Shell program).

3.4 Resulting Software Development

Field-state vectors of the modal equations (EQ 17) are processed by stand alone program modules called (*single-field*) *analyzers*. The solution of the modal equations (EQ 17) results from the execution of a set of *filters* and *field analyzers* operating in sequential or parallel fashion. Figure 3 is a short layout of the overall interfacing software. Filters and field analyzers are communicating and co-existing within a Korn Shell script. The Korn Shell is an interactive command and programming language available in UNIX, HP-UX, MS-DOS and other systems [Olczak; 1992]. The script uses the executable version of the filters and analyzers no matter what languages were used in the individual source codes. No modification of the field analyzers is required for being implemented in the system (except for printing out sufficient data for external communications). The filters are supported FORTRAN or C modules.

4.0 RESULTS AND DISCUSSION

The methodology is applied to a first fan stage. The main objectives of this numerical example are:

(a) To demonstrate its capabilities for a three-dimensional structure analyzer and a quasi-three-dimensional fluid analyzer,

(b) To examine relevant computational issues like the modelling of the contact conditions at the part-span shrouds.

4.1 Case Study: A First Fan Stage

The test rotor has 30 blades with part-span shrouds. The blades have an aspect ratio of 4.8 (Fig. 4). Inlet guide vanes are present upstream and a second fan stage is situated downstream. The selected operating poiot is located at the intersection of the mean speed line and the mean operating line of the engine. The rotor speed is 7500 rpm. The pressure ratio is 1.62. The inlet/outlet aerodynamic conditions were extracted from three-dimensional steady Navier-Stokes streamline analyses based on engine rig tests.

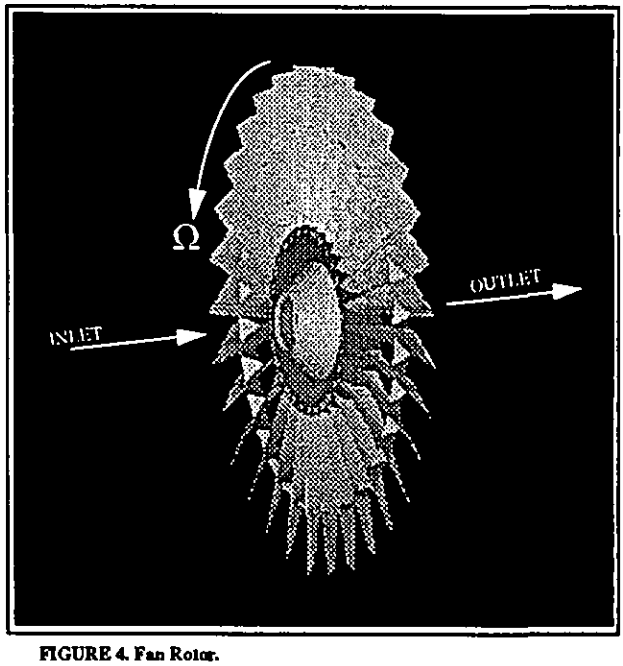

FIGURE 4. Fan Rotor.

4.2 Steady and Unsteady Aerodynamic Analyses

The flow-field analyzer selected for the present test case is a quasi-three-dimensional linearized potential flow solver [Whitehead and Newton; 1985][Whitehead; 1990]. It is based on a Galerkin finite element discretisation scheme. Extensive validation tests of this code are available (one example is the standard configurations compiled by Bölcs and Fransson [1986]). Although this model is based on the potential flow equations and can handle streamtube thickness but no radius variations along streamlines, it is believed that reasonably accurate results can be obtained for the flow conditions expected at the selected operating point.

Eleven stream-surfaces have been meshed from the blade hub to blade tip. Each mesh is performed in the local two-dimensional (meridional distance, radial×angular distance) coordinate system. The overall mesh contains about 4400 (11×40×10) mesh points and 7084 (11×644) two-dimensional triangular elements (Fig. 5). An average number of 30 chord-wise mesh points are used for the different streamsurfaces. The inlet/outlet relative isentropic Mach number varies (hub-to-tip) from 0.65 to 1.04/0.41 to 0.64. The relative flow incidence varies (hub-to-tip) from 7.6 to 9.9 degrees. The relative flow deviation varies (hub-to-tip) from 10.6 to 0.3 degrees. For numerically fulfilling the outlet flow conditions, significant streamtube contraction factors between 0.97 (blade hub) and 0.77 (blade tip) are used. The contour plots showing the variation of the blade surface isentropic relative Mach number are included as Fig. 6 and Fig. 7. A transonic region is embedded to the suction surface between 20 to 100% span. The three-dimensional passage shock extends on the suction side from 60% span (30% chord) to 100% span (50% chord).

For a given aeroelastic mode, the unsteady aerodynamic pressures are calculated for 11 streamsurfaces, 3 mode shapes in modal basis and 30 travelling wave modes. The average CPU time per unsteady aerodynamic run is around 1 second on an IBM 390. The total running time for 11×3×30 aerodynamic computations is about 17 CPU minutes.

4.3 Static and Dynamic Structural Analyses

The structure analyzer is based on a three-dimensional Galerkin finite element discretisation scheme [Jacquet-Richardet et al.; 1994]. It solves the three-dimensional equations of motion for the static and dynamic analysis of rotating and cyclic symmetric blade-disc-shaft assemblies. The standard centrifugal softening and stiffening effects are included. The gyroscopic effects, which are usually negligible for radial blades alone but significant for disks and shafts, are also modelled. In the static analysis, the geometric nonlinearities are solved with a full Newton-Raphson iterative scheme. In the dynamic analysis, the standard Craig and Bampton modal reduction and synthesis method is used. Validation tests of this code are discussed in Jacquet-Richardet et al. [1994].

The mesh used in the present analysis (Fig. 8) contains 3562 nodes and 520 hexaedral solid elements (20 nodes and quadratic shape functions). The left and right hand side cyclic periodic boundaries each have 261 nodes.

Two sets of boundary conditions are considered, respectively called BCx and BCxyz. The model BCx is defined by the following:

1. All nodes on the part-span shroud contact surface are coupled by cyclic periodicity *in the rotor tangential direction x.*
2. All nodes on the left and right hand side boundaries of the disk are coupled by cyclic periodicity in the *x,y,z* directions.
3. The left and right-hand side boundaries of the blade platform are neither coupled nor constrained.
4. The blade and the disk are connected, as shown by Fig. 9.
5. All connection nodes to the neighbouring stages are clamped (Fig. 8).

In the model BCxyz, the boundary condition 1. is replaced by:

1'. All nodes at the part-span shroud contact surfaces are coupled by cyclic periodicity *in the x,y,z directions.*

The static analysis takes about 200 CPU minutes. The dynamic analysis for 30 travelling waves takes about 2000 CPU minutes. All structural computations were run on an HP 712 computer. The natural frequencies calculated for all travelling wave modes are given in Fig. 10 for both models BCx and BCxyz. A few experimental data points for the second mode are also included. They are in very good agreement with model BCx. Boundary conditions at the part-span shrouds are affecting bending (B) and torsion (T) modes: 1B, 1Ba, 1T, 2B, 3B. In all mode shapes computed with BCx, significant relative motions between the part-span shrouds are observed. Modes 1B (Fig. 11), 1T, 2B, 3B mainly involve motions of the blade tip, i.e. above the part-span shrouds. However the mode 1Ba has quite a different behaviour:

1. In model BCxyz or BCx it involves a motion of the whole blade. Furthermore, the bending direction has a large axial component (Fig. 12).
2. In model BCxyz (continuous shroud) and for increasing nodal diameters, the mode involves in-plane deformations of the part-span shroud. Since part-span shrouds are very stiff in these circumstances, the frequency of mode 1Ba increases rapidly with the number of nodal diameters. Besides large couplings with modes 1T, 2B, 3B occur.
3. In model BCx, because relative axial motions between the shrouds are permitted, the steep increase in frequency of mode 1Ba noticed in model BCxyz does not occur.

4.4 Modal Aeroelastic Analysis

As shown in Fig. 5 and in Fig. 8, structure and fluid meshes do not have the same number of mesh points in the span-wise and chord-wise directions. Aerodynamic meshes do not have the same number of mesh points for all streamsurfaces either. Two interfacing grids each containing 11×30 points are generated on the suction and pressure blade surfaces (Fig. 13).

The run time for the interfacing software (without CPU time spent on pure aerodynamics and structural dynamics) for one aeroelastic mode with 30 travelling waves is about 18 CPU minutes on an IBM 390. In this overall aeroelastic analysis, the structure analyzer turns out to be, by far, the most time consuming element. This tendency can easily be reversed if a more time consuming fluid analyzer is selected (for example, a nonlinear flow solver).

The aeroelastic results (ω^*_{a,β_n} frequency and μ^*_{a,β_n} damping ratio) corresponding to the natural modes 1B, 1Ba and 1T are shown in Fig. 16 to Fig. 21. The waves -n and +n are associated to the inter-blade phase angles $-\beta_n$ and $+\beta_n$, respectively.

It is a good validation tool to compare the calculated aeroelastic damping with the uncoupled aerodynamic damping ratio $\overline{\mu}_{a,\beta_n}$ [Carta; 1967]. This latter is calculated by integrating the blade-to-blade quasi-three-dimensional aerodynamic work from the blade hub to the blade tip for a given natural mode (ω_{a,β_n}, $\{\Phi_{a,\beta_n}\}$). It should be pointed out that the computational effort required for the full-span aerodynamic damping is quite similar to that for the aeroelastic damping in terms of automatic transfer of information between the structure and fluid analyzers. For the present test case, the two damping ratios are in good to excellent agreement for all modes. This is an indication that the natural mode shapes are not significantly modified by the amount of aeroelastic modal coupling. It is usually so for stiff structures like blade-shroud-disk assemblies with well separated natural modes.

Both models BCxyz and BCx predict the modes 1B, 1Ba, 1T as stable for all travelling wave modes. From BCxyz to BCx, the geometry of the stability loop is not significantly modified for mode 1B (Fig. 16 and Fig. 19). It is, however, quite modified for mode 1T (Fig. 18 and Fig. 21). For the mode 1Ba only a comparison of travelling waves $0,\pm1,\pm2,\pm3$ is included. All these observations are direct consequences of the differences in terms of mode shape and frequency between models BCxyz and BCx previously discussed in §4.3. The differences in terms of aeroelastic damping between models BCxyz and BCx for modes 1B and 1T are summarized in Fig. 14 and Fig. 15. The model BCxyz has a clear stabilizing effect on the mode 1T. However it is both stabilizing and destabilizing for the mode 1B. More interesting is that the forward waves +1, +2, +3 of mode 1B, which often cause flutter problems, are destabilized. These tendencies are likely to be different if the contact angle between the shrouds is modified.

For the least stable mode, i.e. 1B/-1, the contour plots showing the blade surface distribution of the Mean Accumulated Power (MAP) are included in Fig. 22 to Fig. 25. The local power at $M(x,y,z)$ for the aeroelastic mode (a,β_n) is defined by:

$$p(M) = \frac{-1}{2\pi/\omega^*_{a,\beta_n}} \times \int_0^{2\pi/\omega^*_{a,\beta_n}} \frac{d}{dt}\vec{\phi}^*_{a,\beta_n}(M,t)\ \hat{p}^*_{a,\beta_n}(M,t)\ \cdot \vec{n}(M,t)\, ds$$

Unstable regions are indicated by positive values of p. Interesting remarks are for mode 1B/-1:

1. It is not obvious if the tip sections are the least stable,
2. The stability or instability is more a global (can be quantified by integrating the work over the blade surfaces) than a local (confined to one or two blade sections) characteristic;
3. The steady state shock position defines one of the boundaries of the unstable region (Fig. 24 and Fig. 25);
4. Although models BCx and BCxyz lead to very much the same aeroelastic damping ratio, they exhibit quite different MAP distributions on the pressure side (Fig. 22 and Fig. 23).

4.5 Uncertainties regarding the case study

The aerodynamic analysis employed is obviously a simplification of the three-dimensional and viscous (sometimes separated) flow conditions in the full-scale machine. However, it is not certain whether a quasi-three-dimensional Navier-Stokes solver would do an overall better job with regard to the aeroelastic damping prediction for that geometry [Sidén and Albråten; 1991]. It is presently undertaken to implement more sophisticated aerodynamic solvers.

Like for the flow-field, there are a number of uncertainties as regards to the accuracy of the structural computation. First, the elastic coupling at the part-span shrouds is very difficult to model and this affects considerably the mode shapes. For this reason, two models were studied. Second, although the calculated frequencies may agree well with the experimental data, it is not absolutely certain what the mode shapes will be.

5.0 CONCLUSIONS

A fluid-structure coupling methodology has been presented which provides computational efficiency, flexibility and therefore user's convenience. The following issues have been discussed:

1. The problem of non-matching fluid-structure interface is addressed by working with modal quantities calculated on an interfacing grid.
2. A Korn Shell program has been developed which automates the transfer of data between several fluid and structure analyzers. The implementation of new analyzers in the program is possible within a short time.

The following benefits are gained:

1. One or several user(s) is (are) allowed to work independently on validating the single fluid and structure analyses.
2. Such an approach does not put any constraint on program developments of the individual fluid or structure analyzers.

An aeroelastic analysis carried out on a first shrouded-fan stage was presented. The aeroelastic damping based on the modal coupling scheme and the full-span aerodynamic damping based on stacked quasi-three-dimensional uncoupled analyses are in good agreement for all modes. The results also show the strong dependence of the structure dynamics and aeroelastic damping on the boundary conditions used at the part-span shrouds.

Further developments of the coupled field methodology and the software will involve:

1. The use of different quasi-three-dimensional solvers or processors for different streamlines in the aerodynamic analysis in order to optimize computer time versus accuracy;
2. The development of a modal aeroelastic analysis scheme with structural and aerodynamic mistuning; and
3. The development of a modal forced response analysis scheme with multi-stage structure and fluid analyzers.

ACKNOWLEDGMENTS

Acknowledgements are made to Rolls-Royce plc. (England) for permission to use FINSUP, and Volvo Aero Corporation (Sweden) for providing the test geometry. Special thanks go to Dr. P.

Stow at Rolls-Royce and J.-E. Andreasson, Dr. P. Groth, L. Kjellén, H. Mårtensson at Volvo Aero Corporation. Mr. A. Krainer at the Chair of Heat and Power Technology, Royal Institute of Technology, is also gratefully acknowledged for his encouragement, stimulating discussions, and technical support during this work.

REFERENCES

Appa, K., 1989, "Finite-Surface Spline", *Journal of Aircraft, Vol. 26, No. 5, pp.495-496.*

Bendiksen, O.O., 1990, "Aeroelastic Problems in Turbomachines", *AIAA Paper 90-1157-CP.*

Bendiksen, O.O., 1991, "A New Approach to Computational Aeroelasticity", *Paper AIAA-91-0939-CP.*

Bendiksen, O.O., 1994, "Eulerian-Lagrangian Simulations of Transonic Flutter Instabilities", *Aeroelasticity and Fluid Structure Interaction Problems, AD-Vol. 44, ASME 1994.*

Bölcs, A., and Fransson, T.H., 1986, "Aeroelasticity in Turbomachines: Comparison of Theoretical and Experimental Cascade Results", *Communication du Laboratoire de Thermique Appliquée et de Turbomachines No. 13, EPFL, Switzerland.*

Carta, F.O., 1967, "Coupled Blade-Disk-Shroud Flutter Instabilities in Turbojet Engine Rotors", *ASME Journal of Engineering and Power, July 1967, pp. 420-426.*

Crawley, E.F., 1984, "Aeroelastic Formulations for Turbomachines and Propellers", *Symposium on Unsteady Aerodynamics of Turbomachines and Propellers, Cambridge, England, September 1984, pp. 13-28.*

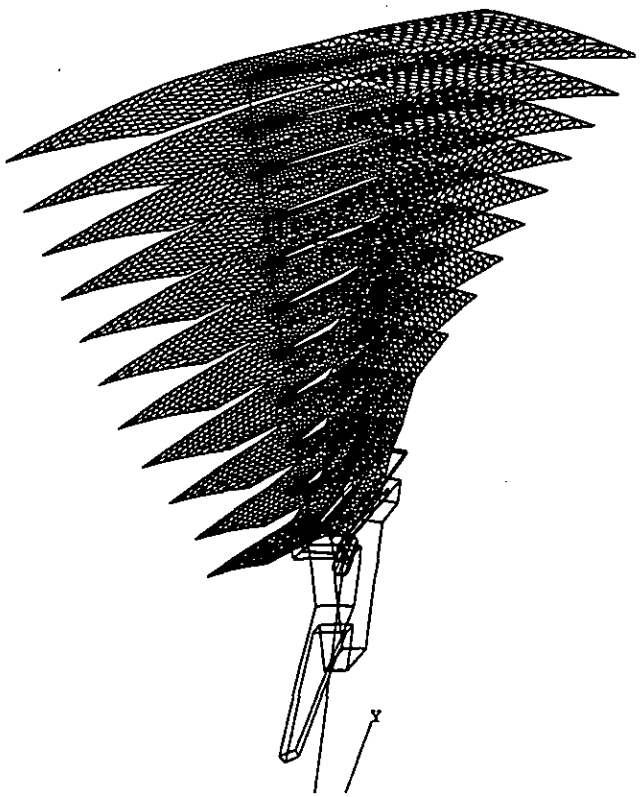

FIGURE 5. Aerodynamic meshes G_a.

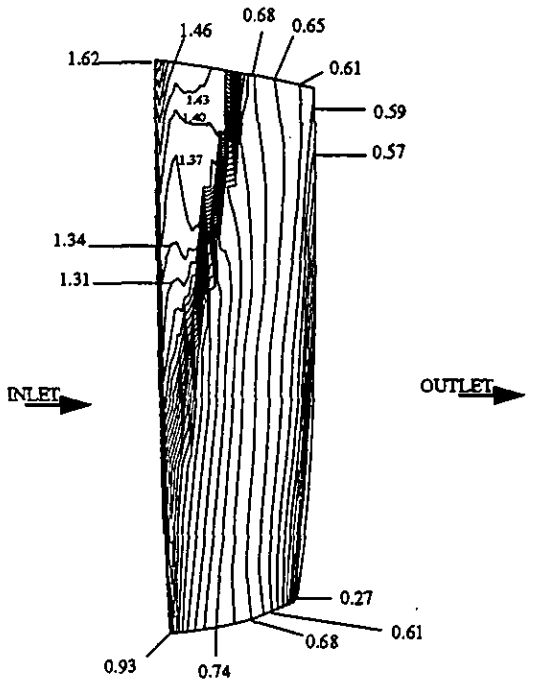

FIGURE 6. Isentropic Mach number contours, suction side.

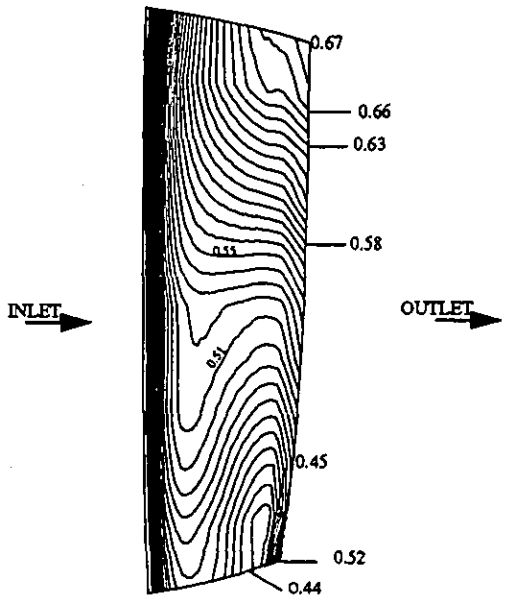

FIGURE 7. Isentropic Mach number contours, pressure side.

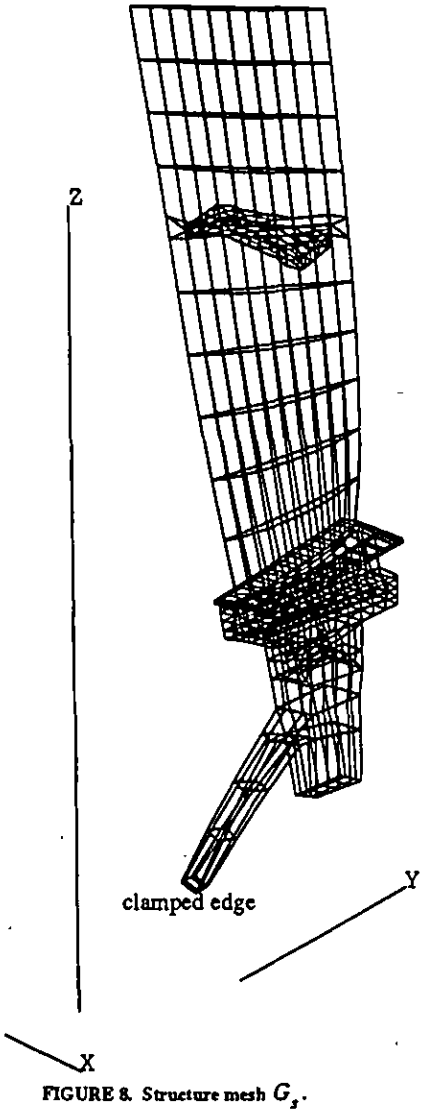

FIGURE 8. Structure mesh G_s.

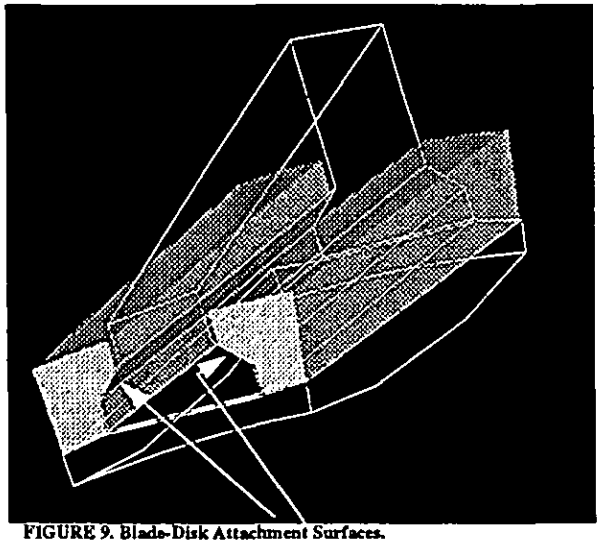

FIGURE 9. Blade-Disk Attachment Surfaces.

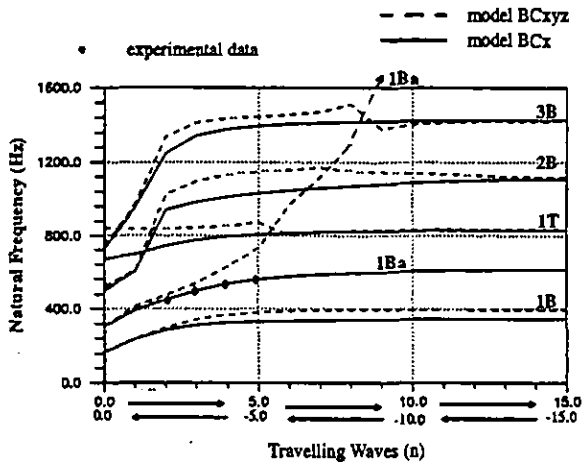

FIGURE 10. Structure natural frequencies as a function of the nodal diameter.

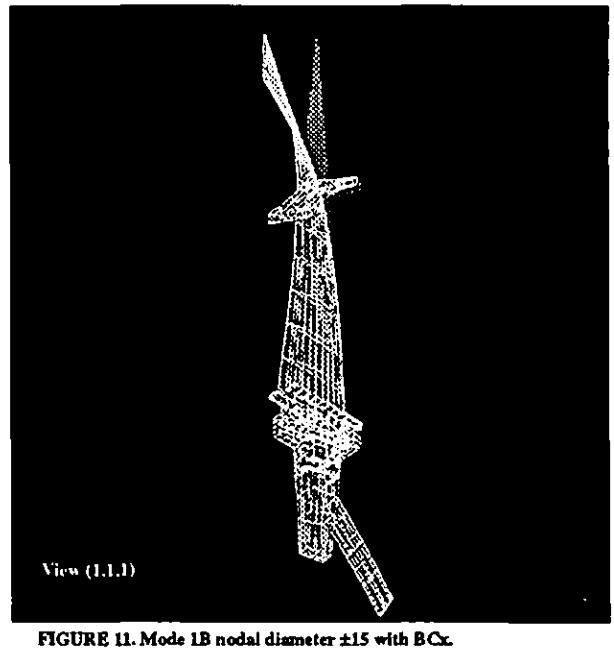

FIGURE 11. Mode 1B nodal diameter ±15 with BCx.

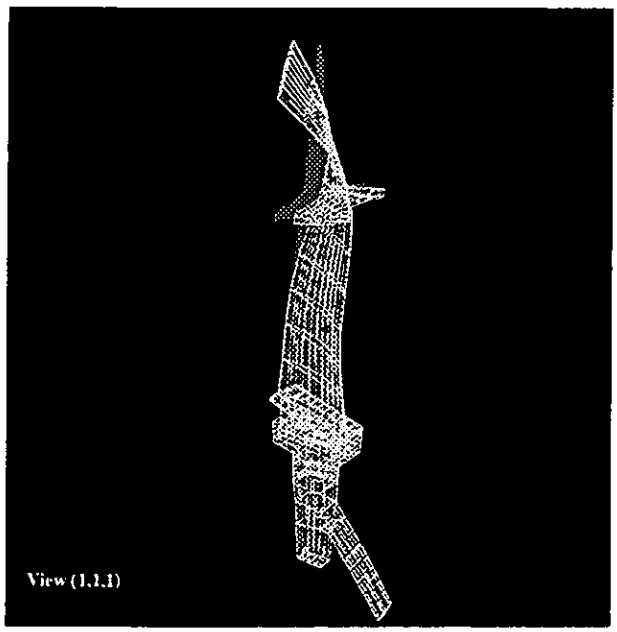

FIGURE 12. Mode 1Ba nodal diameter ±15 with BCx.

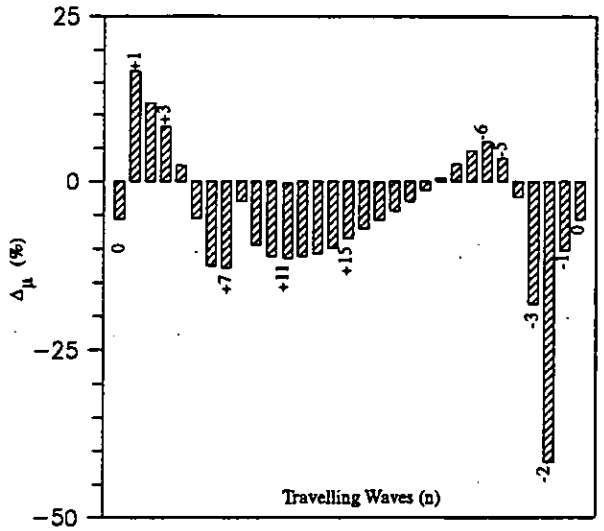

FIGURE 14. Mode 1B, discrepancies for the aeroelastic damping between model BCx and BCxyz, i.e. (BCxyz-BCx)/BCx.

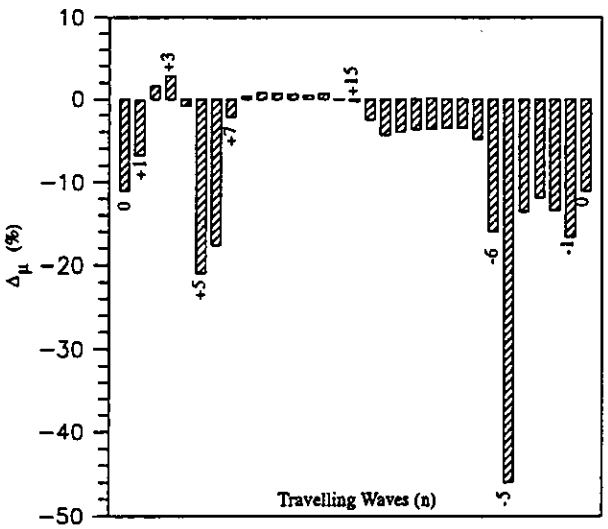

FIGURE 15. Mode 1T, discrepancies for the aeroelastic damping between model BCx and BCxyz, i.e. (BCxyz-BCx)/BCx.

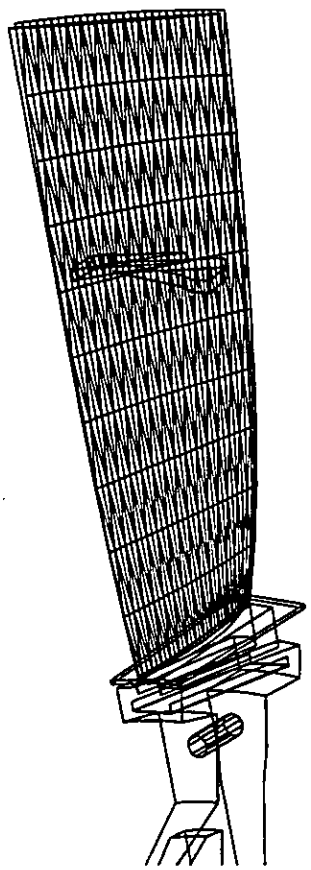

FIGURE 13. Interfacing grid G_i.

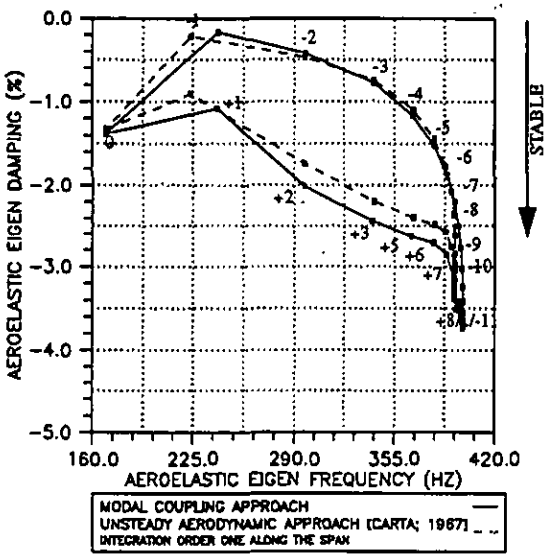

FIGURE 16. Aeroelastic mode 1B, model BCxyz

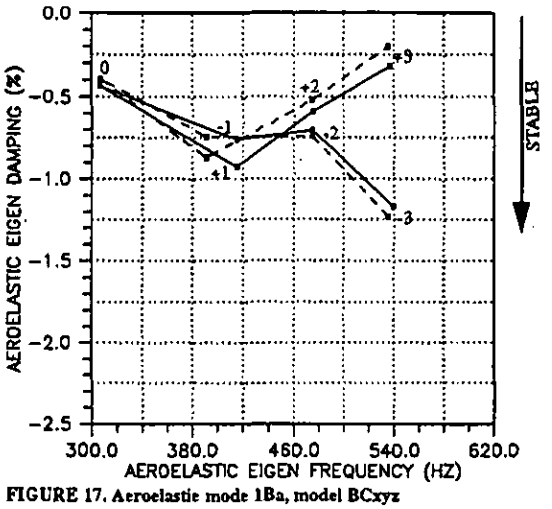

FIGURE 17. Aeroelastic mode 1Ba, model BCxyz

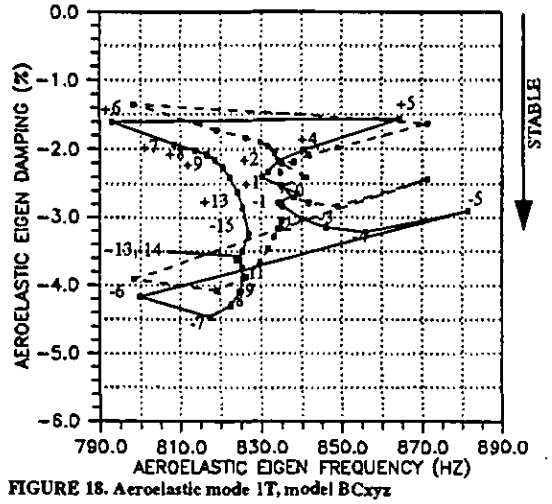

FIGURE 18. Aeroelastic mode 1T, model BCxyz

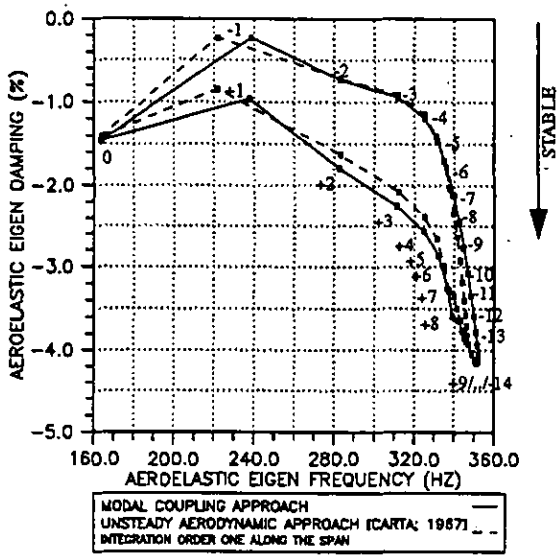

FIGURE 19. Aeroelastic mode 1B, model BCx

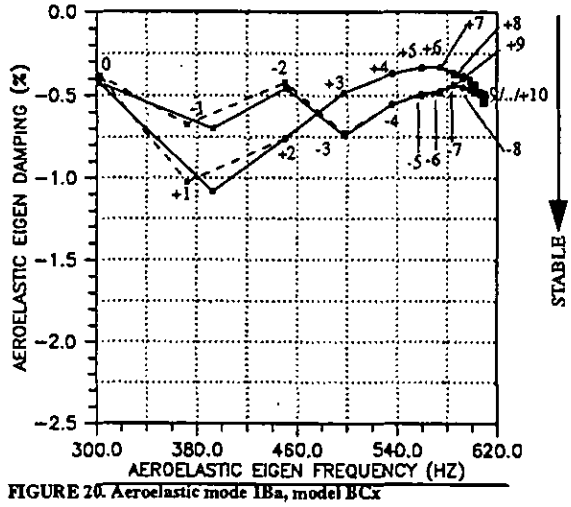

FIGURE 20. Aeroelastic mode 1Ba, model BCx

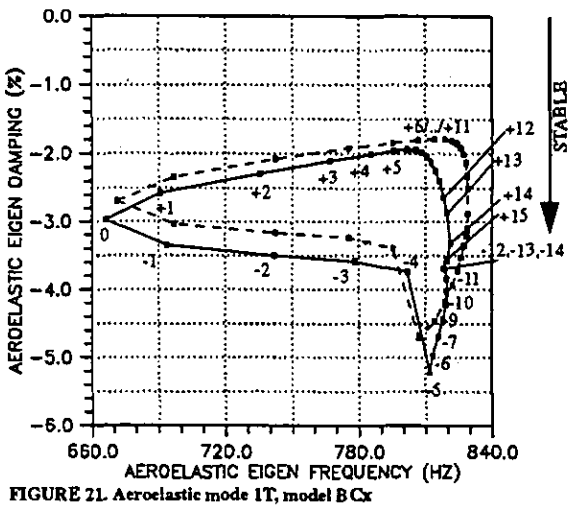

FIGURE 21. Aeroelastic mode 1T, model BCx

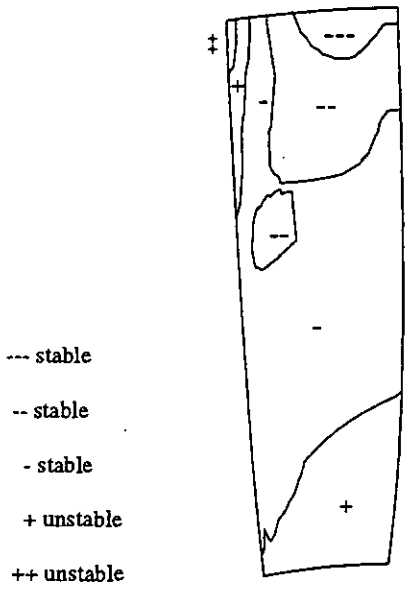

FIGURE 22. MAP contours for mode 1B/-1, model BCxyz, pressure surface.

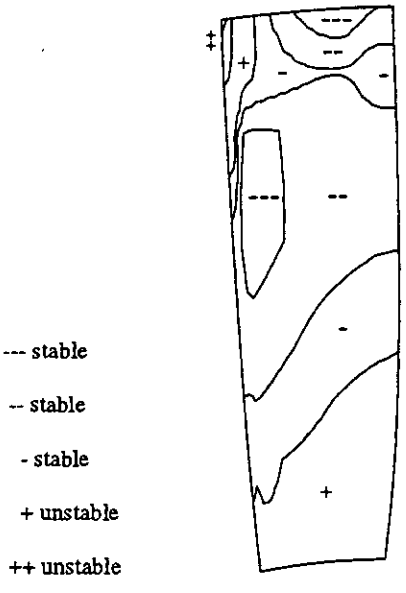

FIGURE 23. MAP contours for mode 1B/-1, model BCx, pressure surface.

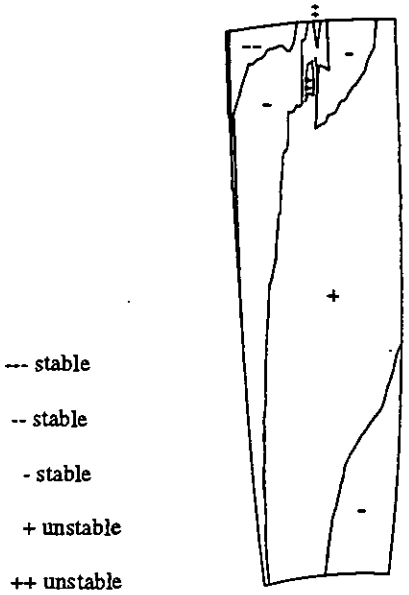

FIGURE 24. MAP contours for mode 1B/-1, model BCxyz, suction surface.

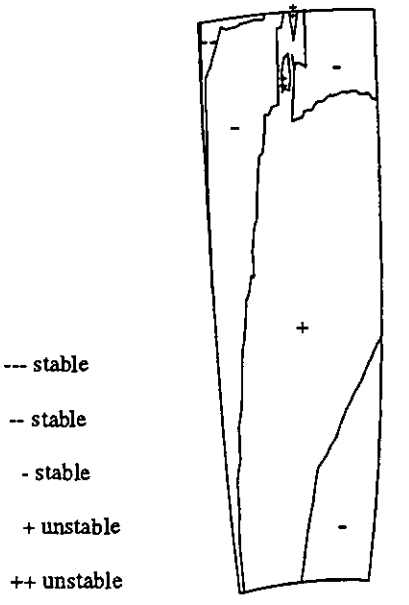

FIGURE 25. MAP contours for mode 1B/-1, model BCx, suction surface.

References (continued)
Gerolymos, G.A., 1993, "Coupled Three-dimensional Aeroelastic Stability Analysis of Bladed Disks", *ASME Journal of Turbomachinery, Vol. 1115, pp. 791-799.*
Gerolymos, G.A., and Vallet, I., 1994, "Validation of 3-D Euler Methods for Vibrating Cascade Aerodynamics", *ASME Paper 94-GT-294.*
Guruswamy, G.P., 1989, "Integrated Approach for Active Coupling of Structures and Fluids", *AIAA Journal, Vol. 27, No. 6, 1989, pp. 788-793.*
Hall, K.C., and Lorence, C.B., 1993, "Calculations of Three-Dimensional Unsteady Flows in Turbomachinery Using the Linearized Harmonic Euler. Equations", *ASME Journal of Turbomachinery, Vol. 115, pp. 800-809.*
He, L., 1994, "Integration of 2-D Fluid/Structure Coupled System for Calculations of Turbomachinery Aerodynamic/Aeroelastic Instabilities", *Computational Fluid Dynamics, Vol. 3, pp. 217-231.*
Henry, R., and Vincent, B., 1990, "Instabilité Aéroélastique dans les Moteurs d'Avions—Application à un étage de Souffiante SNECMA," *Revue Francaise de Mécanique, Vol. 1990.0, pp. 23-32.*
Imregun, M., 1995, "Prediction of Flutter Stability Using Aeroelastic Frequency Response Functions", *Journal of Fluid and Structures, Vol. 9, pp. 419-434.*
Jacquet-Richardet, G., and Henry, R., 1994, "A Modal Aeroelastic Finite Element Analysis Method For Advanced Turbomachinery Stages", *International Journal For Numerical Methods in Engineering, Vol. 37, pp. 4205-4217.*
Jacquet-Richardet, G., Ferraris, G., and Rieutord, P., 1994, "Frequencies and Modes of Rotating Flexible Bladed-Disc-Shaft Assemblies: A Global Cyclic Symmetric Approach", *To be published in the Journal of Sound and Vibration.*
Kielb, R.E., and Kaza, K.R.V., 1984, "Effects of Structural Coupling on Mistuned Cascade Flutter and Response", *ASME Journal of Engineering for Gas Turbines and Power", Vol. 106, pp. 17-24.*
Marshall, J.G., Imregun, M., 1995, "A 3D Time-Domain Flutter Prediction Method For Turbomachinery Blades", *published at the Royal Aeronautical Science Society Meeting, Manchester, England, June 1995.*
Olczak, A., 1992, "The Korn Shell", *Addison-Wesley Publishing Company, 384 pages.*
Sidén, L.D., Albråten P.J., 1991, "A Flutter of a Two-dimensional Transonic Fan Blade Configuration", *presented at the Tenth Symposium on Air Breothing Engines, Nottingham, England, September 1991.*
Smith, T.E., 1991, "A Modal Aeroelastic Analysis Scheme for Turbomachinery Blading", *NASA-CR-187089, 132 pages.*
Srinivasan, A.V., and Fabunmi, J.A., 1984, "Cascade Flutter Analysis of Cantilever Blades", *ASME Journal of Engineering for Gas Turbines and Power, Vol. 106, pp. 34-43.*
Thomas, D.L., 1979, "Dynamics of Rotationally Periodic Structures", *International Journal for Numerical Methods in Engineering, Vol. 14, pp. 81-102.*
Vadhati, M., and Imregun, M., 1994, "Nonlinear Aeroelasticity Analyses using Unstructured Meshes", *Unsteady Aerodynamics and Aeroelasticity of Turbomachines, Edited by Y. Tanida and M. Namba, Elsevier Science.*
Whitehead, D.S., Newton, S.G., 1985, "A Finite Element Method for the Solution of Two-dimensional Transonic Flows in Cascades", *International Journal for Numerical Methods in Fluids, Vol. 5, pp. 115-132.*
Whitehead, D.S., 1990, "A Finite Element Solution of Unsteady Two-dimensional Flow in Cascades", *International Journal for Numerical Methods in Fluids, Vol. 10, pp. 13-34.*